

Article

Microstructure and Mechanical Properties of Diffusion-Bonded CoCrNi-Based Medium-Entropy Alloy to DD5 Single-Crystal Superalloy Joint

Shiwei Li ^{1,2}, Xianjun Sun ^{1,2}, Yajie Du ^{1,2}, Yu Peng ^{1,2}, Yipeng Chen ^{1,2}, Zhaoxi Li ^{1,2}, Jiangtao Xiong ^{1,2,*} 
and Jinglong Li ^{1,2,*}

¹ State Key Laboratory of Solidification Processing, Northwestern Polytechnical University, Xi'an 710072, China; lisw@mail.nwpu.edu.cn (S.L.); 2019260981@mail.nwpu.edu.cn (X.S.); duyajie@mail.nwpu.edu.cn (Y.D.); pengyuyu@mail.nwpu.edu.cn (Y.P.); 2019200858@mail.nwpu.edu.cn (Y.C.); zxli@mail.nwpu.edu.cn (Z.L.)

² Shaanxi Key Laboratory of Friction Welding Technologies, Northwestern Polytechnical University, Xi'an 710072, China

* Correspondence: xiongjiangtao@nwpu.edu.cn (J.X.); lijinglg@nwpu.edu.cn (J.L.)

Abstract: This study focuses on the diffusion bonding of a CoCrNi-based medium-entropy alloy (MEA) to a DD5 single-crystal superalloy. The microstructure and mechanical properties of the joint diffusion-bonded at variable bonding temperatures were investigated. The formation of diffusion zone, mainly composed of the Ni₃(Al, Ti)-type γ' precipitates and Ni-rich MEA matrix, effectively guaranteed the reliable joining of MEA and DD5 substrates. As the bonding temperature increased, so did the width of the diffusion zone, and the interfacial microvoids significantly closed, representing the enhancement of interface bonding. Both tensile strength and elongation of the joint diffusion-bonded at 1110 °C were superior to those of the joints diffusion-bonded at low temperatures (1020, 1050, and 1080 °C), and the maximum tensile strength and elongation of 1045 MPa and 22.7% were obtained. However, elevated temperature produced an adverse effect that appeared as grain coarsening of the MEA substrate. The ductile fracture of the joint occurred in the MEA substrate (1110 °C), whereas the tensile strength was lower than that of the MEA before diffusion bonding (approximately 1.3 GPa).

Keywords: microstructure; mechanical properties; medium-entropy alloy; single-crystal superalloy; diffusion bonding



Citation: Li, S.; Sun, X.; Du, Y.; Peng, Y.; Chen, Y.; Li, Z.; Xiong, J.; Li, J. Microstructure and Mechanical Properties of Diffusion-Bonded CoCrNi-Based Medium-Entropy Alloy to DD5 Single-Crystal Superalloy Joint. *Crystals* **2021**, *11*, 1127. <https://doi.org/10.3390/cryst11091127>

Academic Editor: Cyril Cayron

Received: 27 August 2021

Accepted: 11 September 2021

Published: 16 September 2021

Publisher's Note: MDPI stays neutral with regard to jurisdictional claims in published maps and institutional affiliations.



Copyright: © 2021 by the authors. Licensee MDPI, Basel, Switzerland. This article is an open access article distributed under the terms and conditions of the Creative Commons Attribution (CC BY) license (<https://creativecommons.org/licenses/by/4.0/>).

1. Introduction

High-entropy alloys (HEAs), consisting of four or more elements with each concentration between 5 and 35 at.%, exhibit various composition designs, interesting phase transformations, and noble properties. HEAs have been receiving extensive research focus since the conception of HEA was proposed [1–3]. Among these, HEAs with a face-centered cubic (FCC) structure, represented by the CoCrFeMnNi family, have been attracting the most attention during the past decade [4,5]. CoCrNi medium-entropy alloys (MEAs) with low stacking fault energy (SFE) were optimized from CoCrFeMnNi HEAs. The MEAs present a superior combination of strength and ductility because of nanoscale twins promoting plasticity and continuous hardening [6–8]. Furthermore, CoCrNi-based MEAs containing coherent nanoscale γ' phase with an L12 superlattice structure, namely ordered FCC structure, are potentially advantageous materials to compete with commercial superalloys [9,10]. According to An et al. [10], a CoCrNi-based MEA composed of Ni₃(Al, Ti, Ta)-type γ' precipitates and γ matrix processes a strength–ductility combination both at room temperature and 700 °C (more outstanding than the performance of IN718 superalloys) and unifies the complementary advantages of commercial solid-solution- and precipitation-strengthened superalloys. Consequently, L12-strengthened CrCoNi-based

MEAs are reasonably expected to be structural materials partly replacing commercial superalloys for potential engineering applications. Similarly, Ni-based single-crystal superalloys produced by directional solidification (DS) are suitable for engineering applications with extreme requirements due to their satisfactory high-temperature strength and outstanding creep and oxidation resistance [11–13]. The proximity of CrCoNi-based MEAs and Ni-based single-crystal superalloys in composition, performance, and applicable environment makes the joining of MEAs and single-crystal superalloys highly anticipated for engineering applications. In addition, the reliable joining of MEAs/single-crystal superalloys can achieve complementary superiorities of both materials, significantly extending the potential applications in areas such as the aviation industry, aerospace engineering, and nuclear energy engineering [14,15].

Welding, an irreplaceable metal forming method, plays a pivotal role in the practical applications of emerging HEAs and MEAs. Recently reported welding methods include fusion welding [16], friction welding [17,18], brazing [19,20], transient liquid phase bonding [15], and diffusion bonding [21–23]. Diffusion bonding, a solid-state welding technology, exhibits exceedingly good adaptability to advanced structural materials and hardly damages the performance of base metal. In particular, diffusion bonding is a priority for realizing a sound joint of dissimilar materials, which greatly relieves the problems such as poor compatibility, residual stresses, and thermal cracks [24,25]. Diffusion bonding of AlCoCrFeNi_{2.1} HEA to GH4169 superalloy and TiAl alloy was completed and the microstructural characteristics and mechanical properties were reported by Li et al. [22,23]. However, diffusion bonding of HEAs (or MEAs) to Ni-based single-crystal superalloys has not yet been reported. The interfacial void closure, element diffusion characteristics, effect of bonding parameters on joint performance, and fracture behavior of diffusion-bonded joints are still undefined. Therefore, detailed investigation on diffusion bonding of HEAs (or MEAs) to Ni-based single-crystal superalloys is of significant importance for accelerating the realization of engineering applications.

In this study, the diffusion bonding of CoCrNi-based medium-entropy alloy to DD5 single-crystal superalloy was performed under vacuum. The typical microstructure and microstructural evolution were investigated. The effect of diffusion bonding temperature on the joint performance was evaluated. In addition, the mechanical properties and crack propagation behavior of the joint under tensile test were elucidated.

2. Materials and Methods

The base materials used in this study were (CoCrNi)₉₄Al₃Ti₃ MEA and DD5 single-crystal superalloy. The chemical compositions of DD5 single-crystal superalloy and (CoCrNi)₉₄Al₃Ti₃ MEA are listed in Table 1. The (CoCrNi)₉₄Al₃Ti₃ MEA was self-prepared by arc melting mixed high-purity (greater than 99.95 wt.%) Co, Cr, Ni, Al, and Ti particles under argon protection. The (CoCrNi)₉₄Al₃Ti₃ ingot was remelted four times with electromagnetic stirring and then injected into a rectangular copper mold. The rectangular MEA was treated by homogenization (i.e., 4 h duration at 1200 °C) and then water-quenched. Next, the MEA was cold-rolled to the thickness reduction of 60% along the direction of suction casting. Finally, recrystallization treatment for the rolled sheet was conducted at 1150 °C for 1.5 min to produce equiaxed grains, followed by aging at 800 °C for 2 h. The DD5 single-crystal superalloy was manufactured by DS along [001] orientation and was solution-treated at 1300 °C for 2 h followed by air cooling. Thereafter, the DD5 was aged at 1120, 1080, and 900 °C for 4 h and air-cooled.

Figure 1 shows the microstructure of the (CoCrNi)₉₄Al₃Ti₃ and DD5 before diffusion bonding. The (CoCrNi)₉₄Al₃Ti₃ is composed of Ni₃(Al, Ti)-type γ' precipitates and γ matrix (Figure 1a,b), consistent with that reported by Zhao et al. [9]. The DD5 contains γ' strengthening phase, γ matrix, and granular carbides mainly distributed in the interdendritic zone, as shown in Figure 1c,d. The (CoCrNi)₉₄Al₃Ti₃ and DD5 for diffusion bonding were cut into cylinders by wire electrical discharge machining with heights of 5 and 15 mm respectively and both diameters of 16 mm. All the bonding surfaces were

polished employing 1500-grit SiC paper to remove oxide films. After that, the samples for diffusion bonding were ultrasonically cleaned in alcohol for 10 min, followed by drying with cold air. Subsequently, the samples were fixed in a vacuum furnace by graphite clamps. The assembly of the sample for diffusion bonding is presented in Figure 2. The diffusion bonding processes were carried out at variable bonding temperatures of 1020, 1050, 1080, and 1110 °C for 1 h. A bonding pressure of 10 MPa was applied to promote void closure, and the vacuum condition was maintained below 6×10^{-3} Pa throughout diffusion bonding.

Table 1. Chemical composition of the DD5 single-crystal superalloy and $(\text{CrCoNi})_{94}\text{Al}_3\text{Ti}_3$ MEA (wt.%).

Base Metals	Co	Cr	Al	Ti	Ta	Hf	Mo	W	Re	B	C	Ni
DD5	7.38	6.96	6.10	-	6.42	0.14	1.42	5.02	3.02	0.003	0.052	63.485
$(\text{CoCrNi})_{94}\text{Al}_3\text{Ti}_3$	33.30	29.34	1.46	2.60	-	-	-	-	-	-	-	33.30

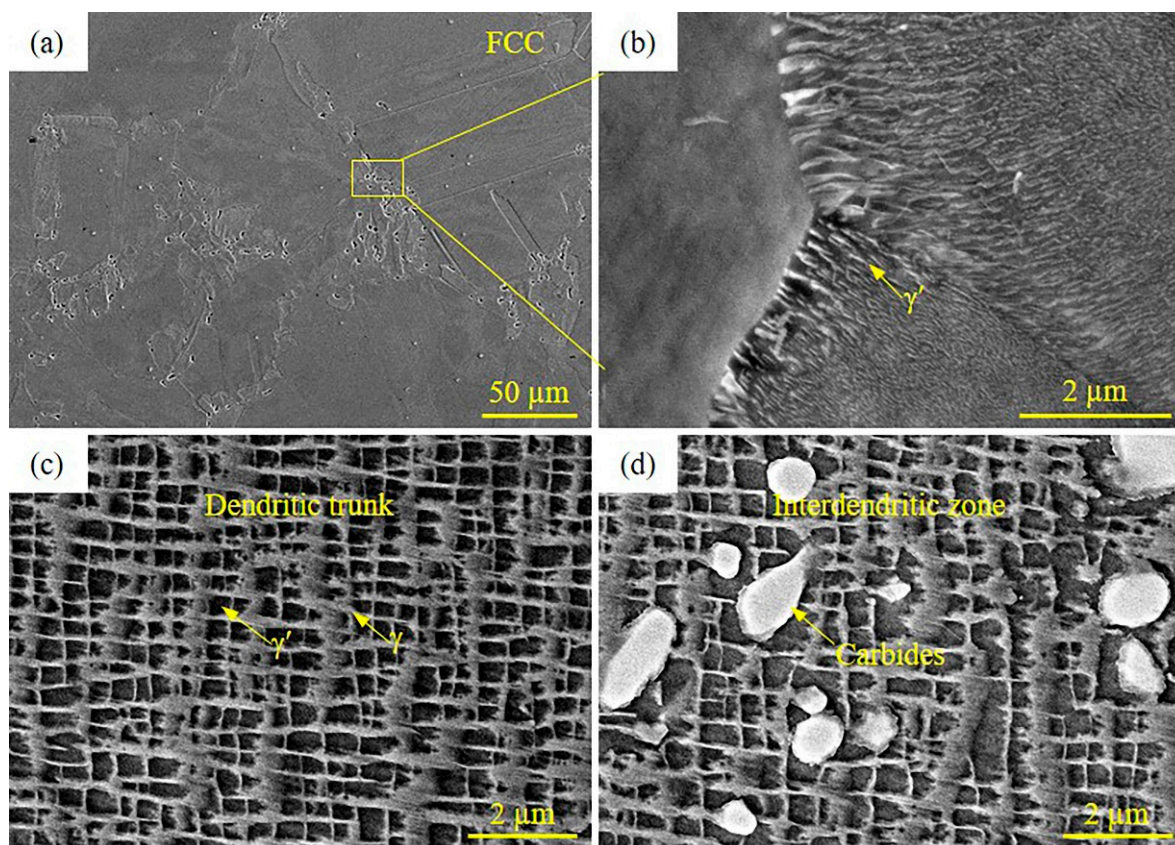


Figure 1. Microstructure of the base materials: (a) $(\text{CoCrNi})_{94}\text{Al}_3\text{Ti}_3$ MEA and (b) corresponding magnified morphology; (c) dendritic trunk and (d) interdendritic zone of DD5 single-crystal superalloy.

The microstructure of the diffusion-bonded joint was examined by scanning electron microscopy (SEM, Helios G4 CX) coupled with energy-dispersive spectroscopy (EDS). The distribution of chemical composition across the MEA/DD5 interface was detected using EDS with a 10 kV accelerating voltage and scanning step of 0.05 μm . The peaks chosen for the Cr, Co, Ni, Al, Ti, Mo, Ta, and W elements were K, L, L, K, K, L, M, and M families, respectively. The mechanical properties of the diffusion-bonded joint were evaluated employing a universal testing machine (Instron 3382). The tensile tests were conducted with a speed of 0.5 mm/min at room temperature.

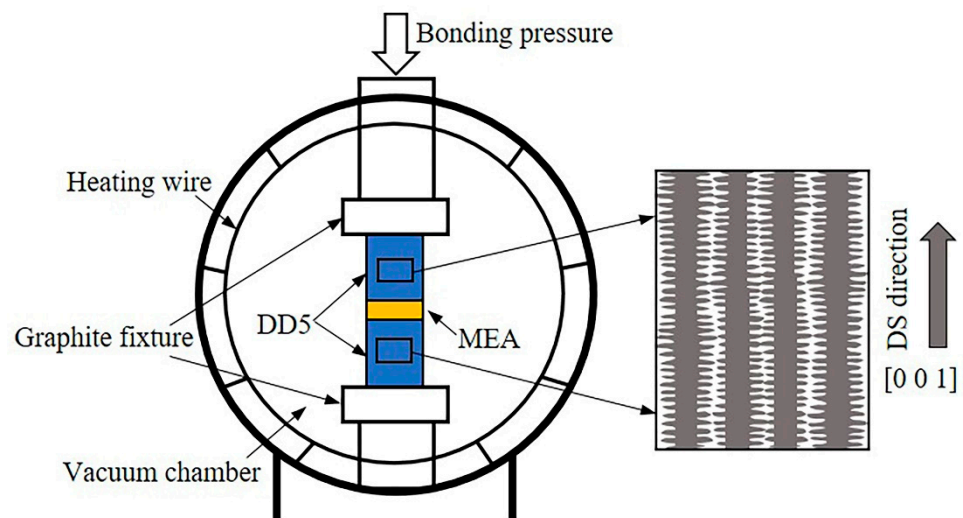


Figure 2. Sketch of the diffusion bonding assembly for $(\text{CoCrNi})_{94}\text{Al}_3\text{Ti}_3$ MEA and DD5 single-crystal superalloy.

3. Results and Discussion

3.1. Typical Microstructure of the Diffusion-Bonded MEA/DD5 Joint

Figure 3 shows the microstructure of the $(\text{CoCrNi})_{94}\text{Al}_3\text{Ti}_3$ MEA to DD5 single-crystal superalloy joint that was diffusion-bonded at $1110\text{ }^\circ\text{C}$ for 1 h. The interfacial microstructure illustrates that overall a sound bonded interface without apparent cracks and voids was obtained under this condition, as shown in Figure 3a. Figure 3b demonstrates the magnified photograph of the bonded interface in Figure 3a. A $6.9\text{ }\mu\text{m}$ thick diffusion zone was formed due to the interdiffusion of interfacial atoms, which was conducive to the realization of reliable joining. In addition, the chemical composition variation across the diffusion-bonded MEA/DD5 interface was clarified using EDS line scan, as presented in Figure 4. According to the EDS results, the matrix of the diffusion zone was mainly composed of Ni, Co, and Cr, and the concentration of Ni was higher than that of Co and Cr, allowing the MEA to be considered as Ni-rich. Simultaneously, DD5 was rich in Al, promoting $\text{Ni}_3(\text{Al, Ti})$ -type γ' formation, diffused from DD5 to MEA at the bonding temperature ($1110\text{ }^\circ\text{C}$), which led to the formation of supersaturated solid solution located in the diffusion zone (Figure 4b). After diffusion bonding duration, nanoscale $\text{Ni}_3(\text{Al, Ti})$ -type γ' phases labeled in Figure 3b were precipitated in the diffusion zone due to a decrease in solubility with temperature reduction. The microstructure efficiently corresponds to the EDS results, which also conforms to the study of Liu et al. [14]. To be clear, the EDS profile does not represent the exact composition profile because of the interaction volume. It is also a fact that the thickness of the diffusion zone obtained by SEM (Figure 3b) effectively corresponds to that measured by EDS (Figure 4), which illustrates that the EDS result is relatively accurate.

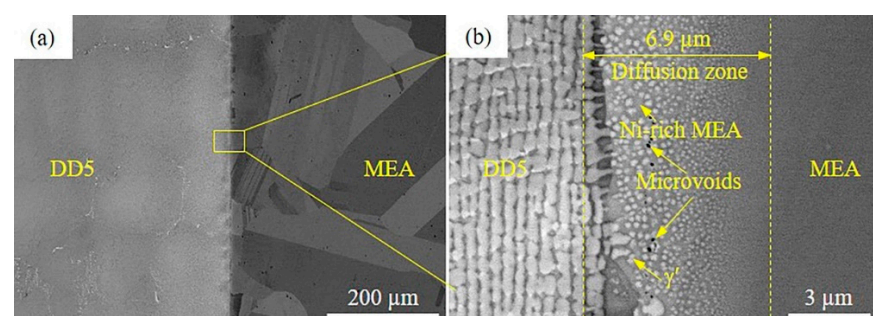


Figure 3. Microstructure of the $(\text{CoCrNi})_{94}\text{Al}_3\text{Ti}_3$ MEA/DD5 single-crystal superalloy joint diffusion-bonded at $1110\text{ }^\circ\text{C}$ for 1 h: (a) interfacial microstructure and (b) corresponding magnified photograph.

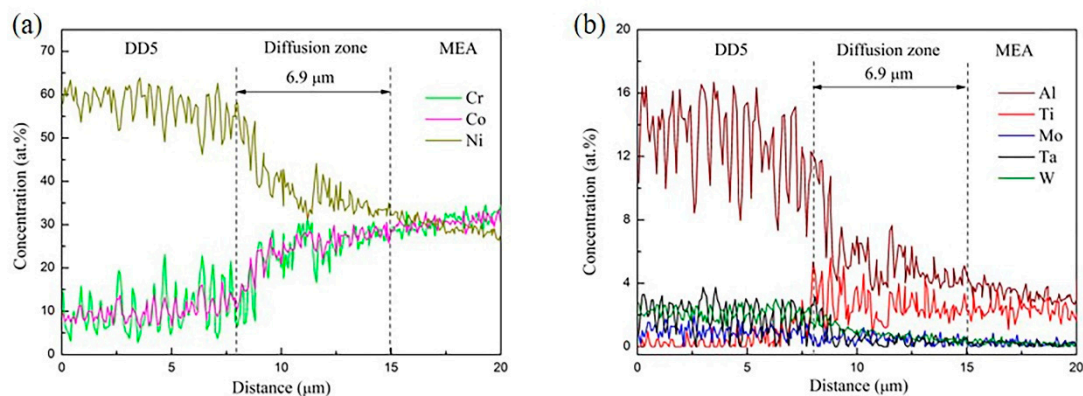


Figure 4. Chemical composition variation across the diffusion-bonded MEA/DD5 interface: (a) Cr, Co, and Ni; (b) Al, Ti, Mo, Ta, and W.

Notably, nanoscale microvoids remained in the diffusion zone of the joint diffusion-bonded at 1110 °C for 1 h, as displayed in Figure 3b. The microvoids were probably due to interfacial porosities (i.e., grinding and polishing imprints) not being completely closed during the bonding duration. In general, interfacial porosities are gradually compacted as a result of interfacial plastic deformation and creep under the combined action of bonding temperature and pressure. The closure of residual microvoids that cannot be compacted by plastic deformation and creep will be dominated by diffusion in the next duration at bonding temperature. If closure of microvoids is not entirely accomplished when diffusion bonding duration is completed, microvoids will remain in the interface of bonded joints [26–28]. Evidently, nanoscale microvoids resided in the bonded joint under this insufficient diffusion bonding condition for complete closure, as observed in Figure 3b.

3.2. Effect of Bonding Temperature on the Microstructure

Figure 5 shows the microstructure of the $(\text{CoCrNi})_{94}\text{Al}_3\text{Ti}_3$ MEA/DD5 single-crystal superalloy joints that were diffusion-bonded at different bonding temperatures (1020, 1050, and 1080 °C) for 1 h. Compared with the joint achieved at 1110 °C (Figure 3), interfacial microvoids were evidently visible in the joints obtained at low bonding temperatures (1020, 1050, and 1080 °C). Reasonably, the dimension and density of microvoids decreased with the increase in bonding temperature due to high temperature reducing the resistance of plastic deformation and creep and promoting the interdiffusion of interfacial atoms. In addition, high temperature assisted the formation of the diffusion zone, principally referring to the diffusion of Ni and Al from the DD5 to the MEA and the diffusion of Co and Cr in the opposite direction. At high bonding temperature (1110 °C), a large amount of Al diffused to the MEA, which resulted in the formation of supersaturated solid solution in the interface region, namely the diffusion zone consisting of γ' precipitates and Ni-rich MEA (Figure 3b). On the contrary, the diffusion zone was blurred in the joints that were diffusion-bonded at low temperatures (1020, 1050, and 1080 °C), as illustrated in Figure 5. Thus, EDS line scan was performed to distinguish the interdiffusion of interfacial atoms. Figure 6 exhibits the elemental distribution across the interface of the joints diffusion-bonded at 1020, 1050, and 1080 °C. Diffusion zones with thicknesses of 3.0, 3.3, and 3.9 μm were formed at 1020, 1050, and 1080 °C respectively, which were significantly thinner than that of 1110 °C (6.9 μm). Notably, some errors are inevitable for EDS results because the volume of emission of the X-rays emitted under the electron beam was ignored.

On the other hand, it is worth noting the effect of bonding temperature on the microstructural evolution of the base metals. It is reasonable to consider that the microstructure of DD5 hardly changed after the bonding processes, in which the bonding temperatures (1020, 1050, 1080, and 1110 °C) were lower than that of aging treatment (1120 °C) and the duration (1 h) was shorter than the aging time (4 h). However, the duration at bonding temperatures led to grain coarsening of the $(\text{CoCrNi})_{94}\text{Al}_3\text{Ti}_3$ MEA in different degrees.

The grain size of the MEA in different states is statistically summarized in Table 2. The grain was significantly coarsened to 232 μm through the bonding process (1 h duration at 1110 $^{\circ}\text{C}$), which was approximately 3.6 times the grain size before diffusion bonding (64 μm).

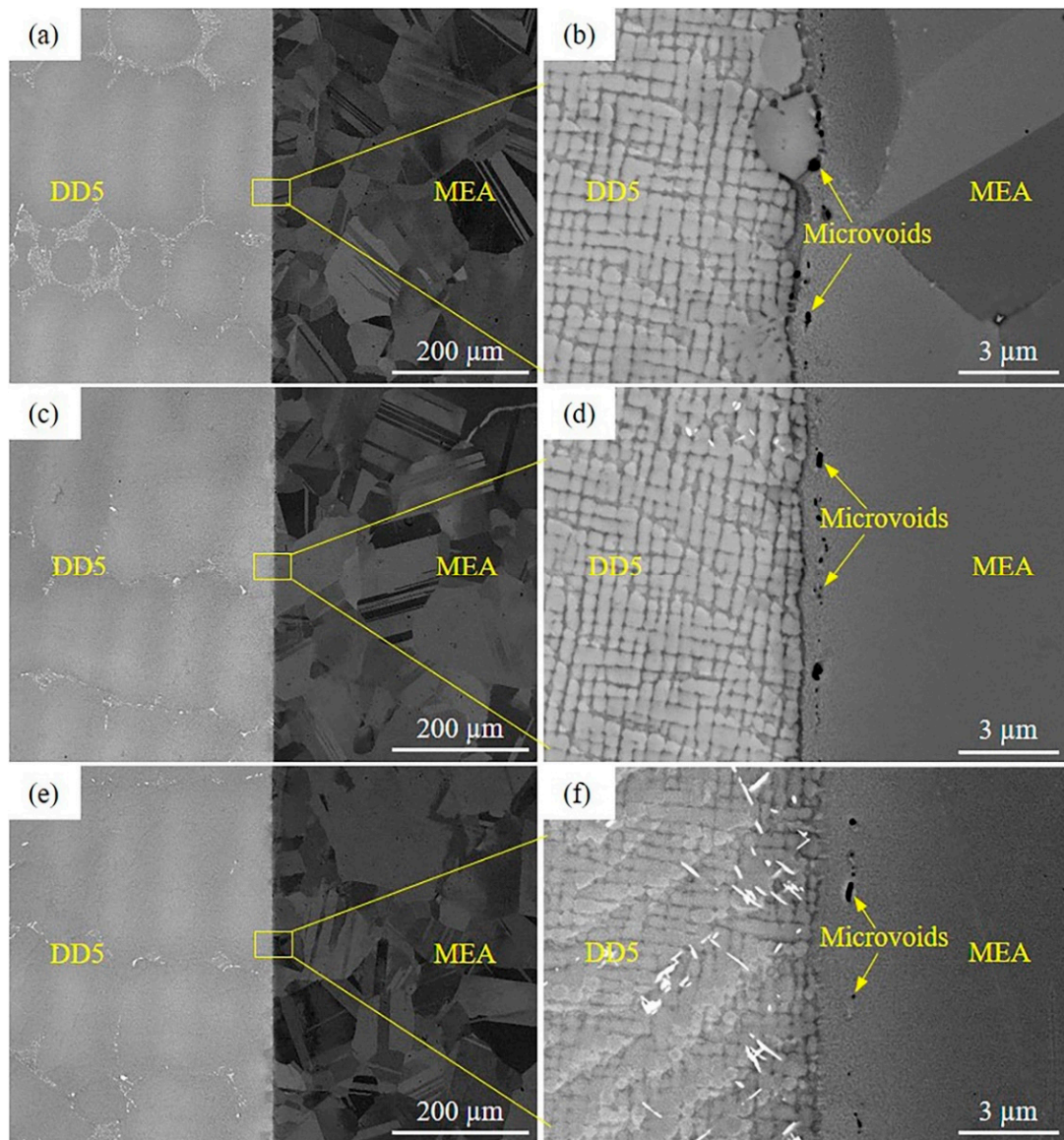


Figure 5. Microstructure of the $(\text{CoCrNi})_{94}\text{Al}_3\text{Ti}_3$ MEA/DD5 single-crystal superalloy joints diffusion-bonded at different temperatures: (a,b) 1020 $^{\circ}\text{C}$, (c,d) 1050 $^{\circ}\text{C}$, and (e,f) 1080 $^{\circ}\text{C}$.

Table 2. Grain size of the $(\text{CoCrNi})_{94}\text{Al}_3\text{Ti}_3$ MEA in different states (μm).

State of the MEA	Before Bonding	Bonded at 1020 $^{\circ}\text{C}$	Bonded at 1050 $^{\circ}\text{C}$	Bonded at 1080 $^{\circ}\text{C}$	Bonded at 1110 $^{\circ}\text{C}$
Grain size	64	95	104	123	232

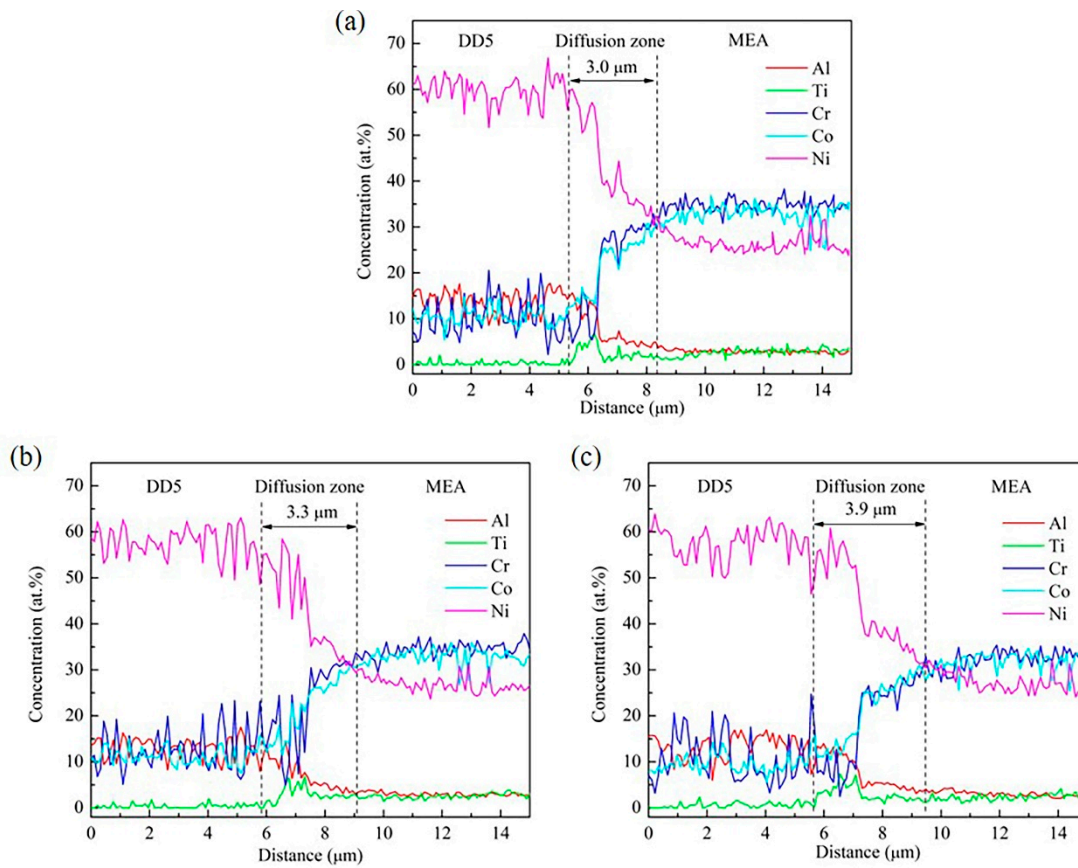


Figure 6. Distribution of chemical composition across the MEA/DD5 interface in the joints diffusion-bonded at different temperatures: (a) 1020 °C, (b) 1050 °C, and (c) 1080 °C.

3.3. Mechanical Properties of the Diffusion-Bonded MEA/DD5 Joint

The mechanical properties of the diffusion-bonded joints were evaluated by tensile tests at 25 °C. Figure 7 shows the tensile strength and elongation of the joints diffusion-bonded at different temperatures. Overall, the joints diffusion-bonded at low bonding temperatures (1020, 1050, and 1080 °C) exhibit similar mechanical properties, including tensile strength and elongation. The tensile strength and elongation are 955 MPa and 14.3% (1020 °C), 968 MPa and 15.2% (1050 °C), 970 MPa and 14.9% (1080 °C), respectively. Comparatively, the joint diffusion-bonded at 1110 °C has superior tensile strength and elongation of 1045 MPa and 22.7%, as illustrated in Figure 7. The apparent microvoids and frail diffusion zones in the joints obtained at low temperatures limited the joint performance [25,29,30]. Both tensile strength and elongation of the joint were improved with bonding temperature elevated to 1110 °C due to high temperature promoting the elimination of microvoids and formation of a sturdy diffusion zone, which sufficiently corresponds to the above microstructural examination.

The fracture behavior and fracture mode of the diffusion-bonded joints were elucidated by macro fracture and magnified surface morphologies. The macro fracture morphologies (flat fracture) demonstrate that the propagation of crack occurred along the MEA/DD5 interface in tensile tests of the joints achieved at 1020, 1050, and 1080 °C (Figure 8a–c). The magnified morphologies of the fracture surface on the MEA side appear as small shallow dimples accompanied by embedded γ' particles (reasonably derived from DD5), indicating a fracture feature occurring in the interface region. Otherwise, the joint was broken in the MEA substrate under tensile load when the joint was diffusion-bonded at 1110 °C (Figure 8d). The MEA part was considered to undergo severe plastic deformation before failure suggested by necking and fibrous zone, and typical ductile dimples were detected on the fracture surface. Consequently, the MEA substrate became the weakest part

of the joint when the sound MEA/DD5 interface was well achieved. Notably, the tensile strength of the MEA after diffusion bonding at 1110 °C for 1 h decreased compared with that of the MEA for bonding (approximately 1.3 GPa) [9], which was attributed to grain growth from 64 to 232 μm . In addition, the tensile elongation of the joint varied greatly from that of a single material sample or a conventional butt joint because the diffusion-bonded sample was assembled into a special sandwich structure.

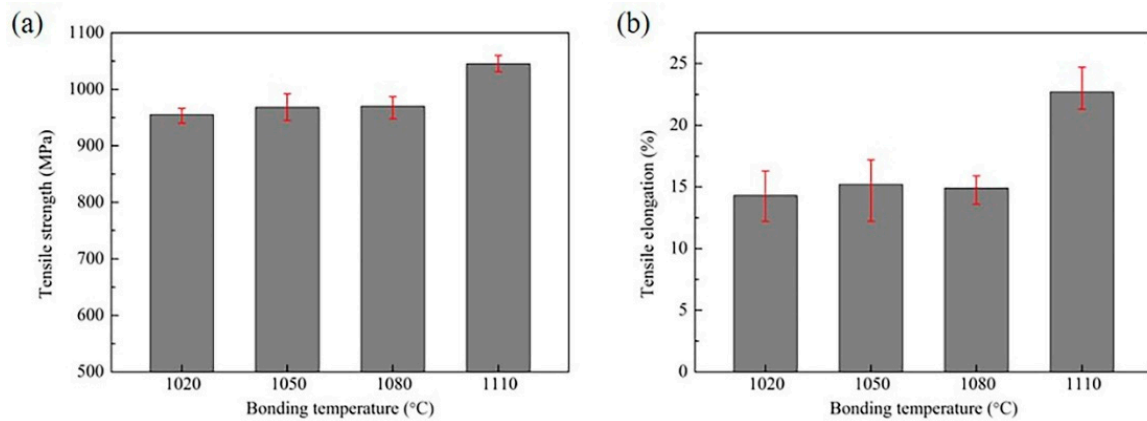


Figure 7. Tensile test results of the joints diffusion-bonded at different temperatures: (a) tensile strength and (b) elongation.

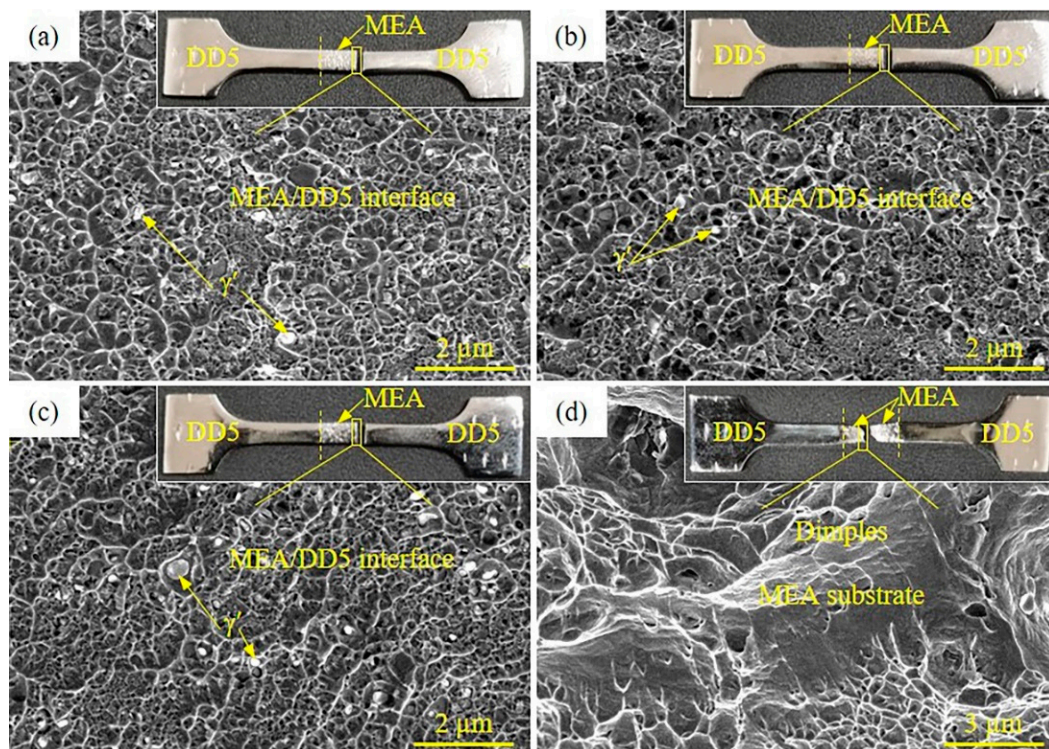


Figure 8. Macro fracture and magnified surface morphologies of the joints diffusion-bonded at (a) 1020 °C, (b) 1050 °C, (c) 1080 °C, and (d) 1110 °C.

4. Conclusions

In this study, the diffusion bonding of CoCrNi-based medium-entropy alloy to DD5 single-crystal superalloy was performed in a vacuum. The microstructure of the diffusion-bonded joint was characterized, and the effect of bonding temperature on the microstructure was elucidated. The mechanical properties and fracture behavior of the joint were evaluated. The following conclusions can be drawn:

(1) The typical diffusion zone with a width of 6.9 μm was formed by diffusion bonding at 1110 $^{\circ}\text{C}$ for 1 h, achieving the reliable joining of MEA and DD5 substrates. The diffusion zone was composed of the $\text{Ni}_3(\text{Al}, \text{Ti})$ -type γ' precipitates and Ni-rich MEA matrix. In addition, nanoscale microvoids remained in the diffusion zone due to the incomplete closure of interfacial porosity.

(2) The width of the diffusion zone increased with the increase in bonding temperature; on the contrary, the size and density of interfacial microvoids decreased. Furthermore, the grain size of MEA substrate significantly grew to 232 μm (diffusion-bonded at 1110 $^{\circ}\text{C}$), which was approximately 3.6 times that of the MEA before diffusion bonding (64 μm).

(3) Both tensile strength and elongation of the joint diffusion-bonded at 1110 $^{\circ}\text{C}$ were superior to those of the joints diffusion-bonded at low temperatures (1020, 1050, and 1080 $^{\circ}\text{C}$). The maximum tensile strength of 1045 MPa and concurrent elongation of 22.7% were achieved when the joint was diffusion-bonded at 1110 $^{\circ}\text{C}$ for 1 h. The typical ductile failure of the joint occurred in the MEA substrate (1110 $^{\circ}\text{C}$), clearly differing from the crack propagating along the MEA/DD5 interface (low temperatures).

Author Contributions: Methodology, S.L., J.X. and J.L.; formal analysis, S.L. and Z.L.; investigation, S.L., Z.L., X.S., Y.D., Y.P. and Y.C.; writing—original draft preparation, S.L.; writing—review and editing, S.L., J.X. and J.L. All authors have read and agreed to the published version of the manuscript.

Funding: This research was funded by National Natural Science Foundation of China, Grant Nos. 51975480, 52075449, and U1737205.

Institutional Review Board Statement: Not applicable.

Informed Consent Statement: Not applicable.

Data Availability Statement: Not applicable.

Conflicts of Interest: The authors declare no conflict of interest.

References

1. Yeh, J.-W.; Chen, S.-K.; Lin, S.-J.; Gan, J.-Y.; Chin, T.-S.; Shun, T.-T.; Tsau, C.-H.; Chang, S.-Y. Nanostructured High-Entropy Alloys with Multiple Principal Elements: Novel Alloy Design Concepts and Outcomes. *Adv. Eng. Mater.* **2004**, *6*, 299–303. [[CrossRef](#)]
2. Zhang, Y.; Zuo, T.T.; Tang, Z.; Gao, M.C.; Dahmen, K.A.; Liaw, P.K.; Lu, Z.P. Microstructures and properties of high-entropy alloys. *Prog. Mater. Sci.* **2014**, *61*, 1–93. [[CrossRef](#)]
3. Miracle, D.; Senkov, O. A critical review of high entropy alloys and related concepts. *Acta Mater.* **2017**, *122*, 448–511. [[CrossRef](#)]
4. Liu, T.; Wu, Z.; Stoica, A.; Xie, Q.; Wu, W.; Gao, Y.; Bei, H.; An, K. Twinning-mediated work hardening and texture evolution in CrCoFeMnNi high entropy alloys at cryogenic temperature. *Mater. Des.* **2017**, *131*, 419–427. [[CrossRef](#)]
5. Shams, S.A.A.; Jang, G.; Won, J.; Bae, J.; Jin, H.; Kim, H.; Lee, C. Low-cycle fatigue properties of CoCrFeMnNi high-entropy alloy compared with its conventional counterparts. *Mater. Sci. Eng. A* **2020**, *792*, 139661. [[CrossRef](#)]
6. Gludovatz, B.; Hohenwarter, A.; Thurston, K.V.S.; Bei, H.; Wu, Z.; George, E.P.; Ritchie, B. Exceptional damage-tolerance of a medium-entropy alloy CrCoNi at cryogenic temperatures. *Nat. Commun.* **2016**, *7*, 10602. [[CrossRef](#)] [[PubMed](#)]
7. Zhang, Z.; Sheng, H.; Wang, Z.; Gludovatz, B.; Zhang, Z.; George, E.; Yu, Q.; Mao, S.X.; Ritchie, R.O. Dislocation mechanisms and 3D twin architectures generate exceptional strength-ductility-toughness combination in CrCoNi medium-entropy alloy. *Nat. Commun.* **2017**, *8*, 14390. [[CrossRef](#)]
8. Laplanche, G.; Kostka, A.; Reinhart, C.; Hunfeld, J.; Eggeler, G.; George, E. Reasons for the superior mechanical properties of medium-entropy CrCoNi compared to high-entropy CrMnFeCoNi. *Acta Mater.* **2017**, *128*, 292–303. [[CrossRef](#)]
9. Zhao, Y.L.; Yang, T.; Tong, Y.; Wang, J.; Luan, J.H.; Jiao, Z.B.; Chen, D.; Yang, Y.; Hu, A.; Liu, C.T.; et al. Heterogeneous precipitation behavior and stacking-fault-mediated deformation in a CoCrNi-based medium-entropy alloy. *Acta Mater.* **2017**, *138*, 72–82. [[CrossRef](#)]
10. An, N.; Sun, Y.; Wu, Y.; Tian, J.; Li, Z.; Li, Q.; Chen, J.; Hui, X. High temperature strengthening via nanoscale precipitation in wrought CoCrNi-based medium-entropy alloys. *Mater. Sci. Eng. A* **2020**, *798*, 140213. [[CrossRef](#)]
11. Li, J.; Jing, J.; He, J.; Chen, H.; Guo, H. Microstructure evolution and elemental diffusion behavior near the interface of Cr₂AlC and single crystal superalloy DD5 at elevated temperatures. *Mater. Des.* **2020**, *193*, 108776. [[CrossRef](#)]
12. Li, P.; Jiang, W.; Rui, S.-S.; Yao, W.-X.; Shi, H.-J.; Han, Q.-N.; Huang, J. Effect of misorientation on the fatigue life of nickel-base single crystal superalloy DD5 at 980 $^{\circ}\text{C}$. *Int. J. Fatigue* **2021**, *153*, 106479. [[CrossRef](#)]
13. Cai, M.; Gong, Y.; Sun, Y.; Qu, S.; Liu, Y.; Yang, Y. Experimental study on grinding surface properties of nickel-based single crystal superalloy DD5. *Int. J. Adv. Manuf. Technol.* **2019**, *101*, 71–85.

14. Liu, J.; Cao, J.; Lin, X.; Song, X.; Feng, J. Microstructure and mechanical properties of diffusion bonded single crystal to polycrystalline Ni-based superalloys joint. *Mater. Des.* **2013**, *49*, 622–626. [[CrossRef](#)]
15. Li, S.; Li, J.; Shi, J.; Peng, Y.; Peng, X.; Sun, X.; Jin, F.; Xiong, J.; Zhang, F. Microstructure and mechanical properties of transient liquid phase bonding DD5 single-crystal superalloy to CrCoNi-based medium-entropy alloy. *J. Mater. Sci. Technol.* **2022**, *96*, 140–150. [[CrossRef](#)]
16. Wu, Z.; David, S.; Feng, Z.; Bei, H. Weldability of a high entropy CrMnFeCoNi alloy. *Scr. Mater.* **2016**, *124*, 81–85. [[CrossRef](#)]
17. Zhu, Z.; Sun, Y.; Ng, F.; Goh, M.; Liaw, P.; Fujii, H.; Nguyen, Q.; Xu, Y.; Shek, C.; Nai, S.; et al. Friction-stir welding of a ductile high entropy alloy: Microstructural evolution and weld strength. *Mater. Sci. Eng. A* **2018**, *711*, 524–532. [[CrossRef](#)]
18. Li, P.; Sun, H.; Wang, S.; Hao, X.; Dong, H. Rotary friction welding of AlCoCrFeNi_{2.1} eutectic high entropy alloy. *J. Alloy. Compd.* **2020**, *814*, 152322. [[CrossRef](#)]
19. Lin, C.; Shiue, R.K.; Wu, S.K.; Lin, Y.S. Dissimilar infrared brazing of CoCrFe(Mn)Ni equiatomic high entropy alloys and 316 stainless steel. *Crystals* **2019**, *9*, 518. [[CrossRef](#)]
20. Li, S.; Li, J.; Shi, J.; Du, Y.; Peng, Y.; Jin, F.; Xiong, J.; Zhang, F. Microstructure and mechanical properties of the brazed region in the AlCoCrFeNi high-entropy alloy and FGH98 superalloy joint. *Mater. Sci. Eng. A* **2020**, *804*, 140714. [[CrossRef](#)]
21. Lei, Y.; Hu, S.; Yang, T.; Song, X.; Luo, Y.; Wang, G. Vacuum diffusion bonding of high-entropy Al_{0.85}CoCrFeNi alloy to TiAl intermetallic. *J. Mater. Process. Technol.* **2020**, *278*, 116455. [[CrossRef](#)]
22. Li, P.; Sun, H.; Wang, S.; Xia, Y.; Dong, H.; Wen, G.; Zhang, H. Diffusion bonding of AlCoCrFeNi_{2.1} eutectic high entropy alloy to GH4169 superalloy. *Mater. Sci. Eng. A* **2020**, *793*, 139843. [[CrossRef](#)]
23. Li, P.; Wang, S.; Xia, Y.; Hao, X.; Dong, H. Diffusion bonding of AlCoCrFeNi_{2.1} eutectic high entropy alloy to TiAl alloy. *J. Mater. Sci. Technol.* **2020**, *45*, 59–69. [[CrossRef](#)]
24. Yuan, L.; Xiong, J.; Peng, Y.; Shi, J.; Li, J. Microstructure and mechanical properties in the solid-state diffusion bonding joints of Ni₃Al based superalloy. *Mater. Sci. Eng. A* **2019**, *772*, 138670. [[CrossRef](#)]
25. Li, S.; Shi, J.; Xiong, J.; Peng, Y.; Ren, J.; Zhang, F.; Li, J. Microstructural characteristics and mechanical properties of WC-Co/steel joints diffusion bonded utilizing Ni interlayer. *Ceram. Int.* **2021**, *47*, 4446–4454. [[CrossRef](#)]
26. Tang, B.; Qi, X.S.; Kou, H.C.; Li, J.S.; Milenkovic, S. Recrystallization Behavior at Diffusion Bonding Interface of High Nb Containing TiAl Alloy. *Adv. Eng. Mater.* **2016**, *18*, 657–664. [[CrossRef](#)]
27. Sun, L.; Li, M. Interfacial voids, microstructure and shear strength of TC4/TC17 bond. *J. Mater. Process. Technol.* **2019**, *270*, 265–273. [[CrossRef](#)]
28. Li, S.-X.; Xuan, F.-Z.; Tu, S.-T. Fatigue damage of stainless steel diffusion-bonded joints. *Mater. Sci. Eng. A* **2008**, *480*, 125–129. [[CrossRef](#)]
29. Li, S.-X.; Xuan, F.-Z.; Tu, S.-T. In situ observation of interfacial fatigue crack growth in diffusion bonded joints of austenitic stainless steel. *J. Nucl. Mater.* **2007**, *366*, 1–7. [[CrossRef](#)]
30. Li, S.-X.; Xuan, F.-Z.; Tu, S.-T.; Yu, S.-R. Microstructure evolution and interfacial failure mechanism in 316LSS diffusion-bonded joints. *Mater. Sci. Eng. A* **2008**, *491*, 488–491. [[CrossRef](#)]